2012 IEEE International Conference on Robotics and Automation
RiverCentre, Saint Paul, Minnesota, USA
May 14-18, 2012

Online Model Estimation of Ultra-Wideband TDOA Measurements for Mobile Robot Localization

Amanda Prorok, Lukas Gonon and Alcherio Martinoli

Abstract— **Ultra-wideband (UWB) localization is a recent technology that promises to outperform many indoor localization methods currently available. Yet, non-line-of-sight (NLOS) positioning scenarios can create large biases in the time-difference-of-arrival (TDOA) measurements, and must be addressed with accurate measurement models in order to avoid significant localization errors. In this work, we first develop an efficient, closed-form TDOA error model and analyze its estimation characteristics by calculating the Cramér-Rao lower bound (CRLB). We subsequently detail how an online Expectation Maximization (EM) algorithm is adopted to find an elegant formalism for the maximum likelihood estimate of the model parameters. We perform real experiments on a mobile robot equipped with an UWB emitter, and show that the online estimation algorithm leads to excellent localization performance due to its ability to adapt to the varying NLOS path conditions over time.**

I. Introduction

Accurate indoor localization is an enabling technology, with applications ranging from asset management and inventory tracking to assembly control for a variety of different industries. Within the research community, the mobile robotics domain plays an important role with a vast and continuously growing body of contributions. Popular localization sensors employed on-board robots include cameras [16], ultrasound sensors [8], laser range finders [17] and even infrared sensors [2], and are used independently or in combination with fixed landmark beacons [3]. Although such systems are proven accurate and efficient, their great disadvantage lies in the requirement for line-of-sight (LOS). Wireless localization signals, in particular those relying on UWB, are able to penetrate through objects in NLOS scenarios due to the large frequency spectrum, and thus alleviate the LOS constraint, ultimately enabling localization over large ranges and in dynamic environments [9]. Nevertheless, such NLOS scenarios may cause biases in the signal propagation times, which ultimately leads to significant localization errors. In order to guarantee reliable and accurate performance, these biases need to be addressed by an UWB measurement model (within the localization algorithm), that is able to accurately capture measurement distributions in mixed LOS/NLOS signal path environments.

In this work, we build upon our previous work [12], where we developed a baseline TDOA measurement model and validated it with real data. By performing a closed-form approximation, we now produce a new, more efficient measurement model. Using this new model, we are able to derive a compact and efficient estimation algorithm that can be employed in batch mode (offline) as well as online, in real-time. A derivation of the CRLB for our model illustrates the achievable lower bound on the variance of any unbiased estimator. Also, given a vector of true model parameters, we compare the estimation performance of our batch and online estimation algorithms. Finally, we perform a real localization experiment using a mobile robot equipped with an UWB emitter, and show that the online model estimator produces excellent localization results.

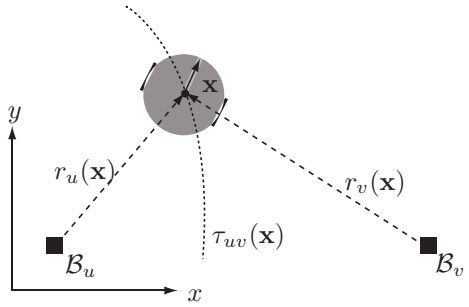

Fig. 1. System of one robot located at $\mathbf{x}$ and two UWB base stations $\mathcal{B}_u$ and $\mathcal{B}_v$. The figure shows the true ranges $r_u(\mathbf{x})$ and $r_v(\mathbf{x})$ to the respective base stations, as well as a segment of the hyperbola resulting from the range-difference measurement $\tau_{uv}(\mathbf{x})$.

A. Related Work

UWB has shown to be amongst the most promising localization techniques for indoor environments [9]. As a consequence, it has very recently been adopted by the robotics community. In [15], an UWB receiver is mounted on a mobile robot which uses a TDOA algorithm between pairs of anchor nodes to estimate its own position. The robot's self-localization algorithm is based on UWB measurements, yet it does not employ an UWB error model, and instead relies on a least squares method to solve the multilateration problem. The studies in [6] and [7] develop probabilistic models for biased UWB range measurements which are combined with on-board odometry data. Yet, both papers model NLOS biases within augmented-state particle filters that do not take LOS/NLOS signal path conditions and bias probability distributions into account explicitly, and might therefore be limited by this simplified approach. To the best of our knowledge, parametric UWB TDOA measurement models have hardly been addressed by the research community. Thus, little work has been done to propose viable model

All authors are with the Distributed Intelligent Systems and Algorithms Laboratory, School of Architecture, Civil and Environmental Engineering at the Ecole Polytechnique Fédérale de Lausanne. The work presented in this paper was supported by the National Competence Center in Research on Mobile Information and Communication Systems (NCCR-MICS), a center supported by the Swiss National Science Foundation under grant number 51NF40-111400. firstname.lastname@epfl.ch

estimators, in particular for applications to mobile robot localization.

B. Problem Formulation

Our problem is illustrated in Figure 1 and is described as follows. We consider a system of two UWB base station receivers $\mathcal{B}_u$ and $\mathcal{B}_v$, each of which is fixed and well-localized in an absolute coordinate system, and one robot at position $\mathbf{x}$ equipped with an UWB emitter tag in its center. At any given time, the robot may receive a measured TDOA value $\hat{\tau}_{uv}$ from the pair of base stations $\langle \mathcal{B}_u, \mathcal{B}_v \rangle$. Thus, we define the TDOA measurement error as the difference between the nominal (error-free) TDOA value τ_{uv} at the actual robot position $\mathbf{x}$ and the measured TDOA value $\hat{\tau}_{uv}$

$$\Delta\tau_{uv}(\hat{\tau}_{uv}, \mathbf{x}) = \hat{\tau}_{uv} - \tau_{uv}(\mathbf{x}) \tag{1}$$

where $\tau_{uv}(\mathbf{x}) = r_u(\mathbf{x}) - r_v(\mathbf{x})$, and $r_u(\mathbf{x})$ is the range between base station $\mathcal{B}_u$ and $\mathbf{x}$. The first goal of this work is to develop an efficient TDOA measurement model $\tilde{p}_{uv}(\Delta\tau_{uv}; \boldsymbol{\theta})$, which is defined by the parameter vector $\boldsymbol{\theta}$. In order to practically employ the model, the second goal of this work is to develop an online estimation algorithm that finds the best estimate $\hat{\boldsymbol{\theta}}$ for the parameter vector $\boldsymbol{\theta}$, and that is sufficiently light to be deployed on a resource-constrained mobile robotic platform.

II. UWB TDOA Measurement Model

UWB is a radio technology which is characterized by its very large bandwidth compared to conventional narrow-band systems, and, in particular, features high positioning accuracy (due to a fine time resolution on both emitter and receiver side) and high material penetrability (due to the large bandwidth). Despite these desirable traits, the resolution of multipath and NLOS signals remains a very hard problem, and may lead to complex time-of-arrival (TOA) detection algorithms prone to estimation errors, which inevitably leads to ranging inaccuracies. In this section, we first develop a baseline error model for TOA measurements, and then extend it analogously to model the errors of TDOA measurements. We note that as of the following, the terms TOA and TDOA are used interchangeably with the terms range and range difference, respectively, as they differ only by a constant factor (propagation speed).

A. General TDOA Measurement Model

We employ a common error model [14] for the range between a base station $\mathcal{B}_u$ and a target node at position $\mathbf{x}$:

$$\hat{r}_u = r_u(\mathbf{x}) + \epsilon + Y b_u \tag{2}$$

where $r_u(\mathbf{x})$ represents the true distance, b_u is a non-negative distance bias introduced by a NLOS signal propagation, and $\epsilon \sim \mathcal{N}(0, \sigma_{\mathcal{N}}^2)$ is a zero-mean Gaussian measurement noise with variance $\sigma_{\mathcal{N}}^2$, common to all base stations. The random variable Y follows a Bernoulli distribution, i.e., it takes the value 1 with probability $(1 - \mathrm{P}_{L_u})$ and the value 0 with probability P_{L_u}, where P_{L_u} is the probability of measuring a LOS path, and correspondingly, $(1 - \mathrm{P}_{L_u})$ is the probability of measuring a NLOS path. Whereas modeling ϵ is straightforward, modeling the bias b_u is less obvious. Indeed, positive time-of-flight biases may not only be caused by multipath propagation, but also by signal delay or by signal attenuation, and thus depend on bandwidth and distance. Despite the complexity of NLOS error patterns, current work discusses the suitability of a variety of statistical models with exponential behavior, supported on the semi-infinite interval $(0, \infty)$ [1, 13]. In particular, Alsindi et al. [1] show in a comprehensive measurement campaign that the log-normal distribution best characterizes the NLOS error behavior. Thus, we resort to a bias b_u that is modeled as a log-normal random variable $b_u \sim ln\mathcal{N}(\mu_u, \sigma_u)$, associated to each base station $\mathcal{B}_u$.

Our TOA measurement model returns the likelihood that a given range error occurs. For a range error defined as

$$\Delta r_u(\hat{r}_u, \mathbf{x}) = \hat{r}_u - r_u(\mathbf{x}) \tag{3}$$

the TOA measurement model describes the likelihood of Δr_u occurring when a robot measures a certain range distance $\hat{r}_u$ from a base station $\mathcal{B}_u$ at an actual position $\mathbf{x}$ with a nominal (actual) range $r_u(\mathbf{x})$. Thus, for a log-normal probability density function $p_{ln\mathcal{N},u}(b_u)$ with parameters μ_u and σ_u, and a normal probability density function $p_{\mathcal{N}}(\epsilon)$ with a standard deviation $\sigma_{\mathcal{N}}$, the probability density of an error Δr_u, occurring in a NLOS event $\bar{L}_u$, can be written as

$$p_u(\Delta r_u | \bar{L}_u) = (p_{ln\mathcal{N},u} * p_{\mathcal{N}})(\Delta r_u) \tag{4}$$

which is the convolution of the probability density function of the bias value, with the probability density function of the Gaussian noise value. Correspondingly, we can write the probability density of an error Δr_u, occurring in a LOS event L_u, as

$$p_u(\Delta r_u | L_u) = p_{\mathcal{N}}(\Delta r_u) \tag{5}$$

Finally, with use of the total probability theorem, we combine the above equations to obtain the probability density of Δr_u (which is obtained by measuring a range $\hat{r}_u$ at an actual, nominal range r_u) as

$$\begin{aligned} p_u(\Delta r_u) = {} & p_u(\Delta r_u | L_u) \cdot \mathrm{P}_{L_u} + \\ & p_u(\Delta r_u | \bar{L}_u) \cdot (1 - \mathrm{P}_{L_u}). \end{aligned} \tag{6}$$

An example of this probability density function is shown in Figure 2(a), for two base stations.

In practice, TOA systems are rarely implemented due to the complexity induced by the required synchronization of a mobile node with the base stations. Instead, it is a common choice to implement TDOA systems which are significantly more practical, since only the synchronization among base stations is required. Thus, the direct range measurement between a mobile node and base station is replaced by the difference between two individual range measurements each taken at a different base station.

Extending the TOA formalism shown above, we define the difference range value (i.e. TDOA) between two base stations $\mathcal{B}_u$ and $\mathcal{B}_v$ to a target node as

$$\hat{\tau}_{uv} = \hat{r}_u - \hat{r}_v \tag{7}$$

Model parameter	μ_u	σ_u	P_{L_u}
Parameter range	[-3,0]	[0.2,0.8]	[0.01,0.99]

TABLE I

MODEL PARAMETER RANGES FOR A BASE STATION $\mathcal{B}_u$

and then easily model the TDOA error $\Delta\tau_{uv}$ as previously shown in Equation 1. Simultaneously, we can describe the TDOA error as the difference between the range errors occurring at the individual base stations $\mathcal{B}_u$ and $\mathcal{B}_v$ as described in Equation 2, resulting in

$$\Delta\tau_{uv} = \Delta r_u - \Delta r_v. \tag{8}$$

Finally, we describe the probability density of a given TDOA measurement error $\Delta\tau_{uv}$ as the probability density of the subtraction of two random variables drawn from the probability densities describing the TOA error models of the two respective base stations. We use the results of Equations 6 to model this resulting probability density as

$$p_{uv}(\Delta\tau_{uv}) = (p_u * p_v^-)(\Delta\tau_{uv}) \tag{9}$$

which is a convolution of the probability densities of range errors Δr_u and Δr_v, and where we denote $p_v^-(\Delta r_v) = p_v(-\Delta r_v)$.

B. Efficient TDOA Measurement Model

Although numerical implementations for the TDOA measurement model of Equation 9 are easily found, they imply nested integrals which may incur a substantial computational overhead when deploying the model on an embedded platform for real-time operation. Also, the model itself is analytically non-tractable, which causes difficulties when deriving viable estimators. For these reasons, we perform a closed-form approximation to simplify the TDOA measurement model of Equation 9. In the following, we will also show that our approximations are easily justified by considering real world UWB data.

Using basic algebraic properties of the convolution and inserting Equation 6 into Equation 9, we have

$$\begin{aligned} p_{uv}(\Delta\tau_{uv}) = \Big(&\mathrm{P}_{L_u}\mathrm{P}_{L_v}(p_{\mathcal{N}} * p_{\mathcal{N}}^-) + \\ &\mathrm{P}_{L_u}(1-\mathrm{P}_{L_v})(p_{\mathcal{N}} * p_{\mathcal{N}}^- * p_{\ln\mathcal{N},v}^-) + \\ &\mathrm{P}_{L_v}(1-\mathrm{P}_{L_u})(p_{\mathcal{N}} * p_{\mathcal{N}}^- * p_{\ln\mathcal{N},u}) + \\ &(1-\mathrm{P}_{L_u})(1-\mathrm{P}_{L_v})(p_{\mathcal{N}} * p_{\mathcal{N}}^- * p_{\ln\mathcal{N},u} * p_{\ln\mathcal{N},v}^-)\Big)(\Delta\tau_{uv}). \end{aligned} \tag{10}$$

It is well-known that $p_{\mathcal{N}} * p_{\mathcal{N}}^- = p_{\sqrt{2}\mathcal{N}}$, where $p_{\sqrt{2}\mathcal{N}}$ is the density of a normal distribution $\mathcal{N}(0, 2\sigma_{\mathcal{N}}^2)$. Hence, Equation 10 can be rewritten as

$$\begin{aligned} p_{uv}(\Delta\tau_{uv}) = \Big(&\mathrm{P}_{L_u}\mathrm{P}_{L_v}p_{\sqrt{2}\mathcal{N}} + \\ &\mathrm{P}_{L_u}(1-\mathrm{P}_{L_v})(p_{\sqrt{2}\mathcal{N}} * p_{\ln\mathcal{N},v}^-) + \\ &\mathrm{P}_{L_v}(1-\mathrm{P}_{L_u})(p_{\sqrt{2}\mathcal{N}} * p_{\ln\mathcal{N},u}) + \\ &(1-\mathrm{P}_{L_u})(1-\mathrm{P}_{L_v})(p_{\sqrt{2}\mathcal{N}} * p_{\ln\mathcal{N},u} * p_{\ln\mathcal{N},v}^-)\Big)(\Delta\tau_{uv}). \end{aligned} \tag{11}$$

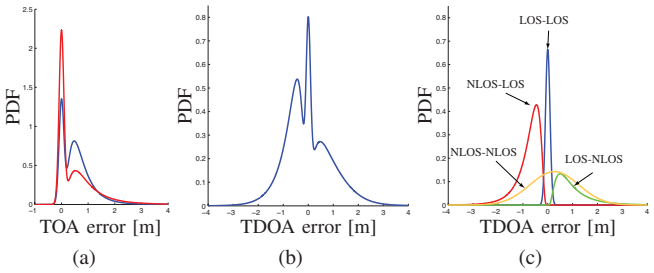

Fig. 2. We consider a base station pair $\langle\mathcal{B}_1, \mathcal{B}_2\rangle$. The plots show an example of the probability density functions describing (a) the TOA error (Eq. 6) for the two base stations and (b) the TDOA error (Eq. 13). Plot (c) illustrates the four modes which form the complete multimodal probability density function shown in (b). The model parameters are set to: $\mu_1 = -0.43$, $\mu_2 = -0.2$, $\sigma_1 = 0.6$, $\sigma_2 = 0.7$, $\mathrm{P}_{L_1} = 0.3$, $\mathrm{P}_{L_2} = 0.5$.

UWB measurement campaigns have shown that $\sigma_{\mathcal{N}} \ll 1$ [1, 12]. Thus $p_{\sqrt{2}\mathcal{N}} * g \approx g$ for any function g. Furthermore (as we will verify numerically later on in this section) $p_{\ln\mathcal{N},u} * p_{\ln\mathcal{N},v}^-$ can be approximated by the density function $p_{\tilde{\mathcal{N}}}$ of a normal distribution $\mathcal{N}(\tilde{\mu}, \tilde{\sigma}^2)$. The parameters $\tilde{\mu}, \tilde{\sigma}^2$ are obtained by matching the moments (and thus minimizing the Kullback-Leibler divergence) as follows: Let $X_u \sim \ln\mathcal{N}(\mu_u, \sigma_u^2)$ and $X_v \sim \ln\mathcal{N}(\mu_v, \sigma_v^2)$ be independent. For the mean $\tilde{\mu}$ and the variance $\tilde{\sigma}^2$, the Kullback-Leibler divergence is minimized if $\tilde{\mu} = \mathrm{E}[X_u - X_v]$ and $\tilde{\sigma}^2 = \mathrm{Var}(X_u - X_v)$. This leads to

$$\begin{aligned} \tilde{\mu} &= \mathrm{E}[X_u - X_v] = e^{\mu_u + \sigma_u^2/2} - e^{\mu_v + \sigma_v^2/2} \\ \tilde{\sigma}^2 &= \mathrm{Var}(X_u) + \mathrm{Var}(-X_v) \\ &= e^{2\mu_u + \sigma_u^2}(e^{\sigma_u^2} - 1) + e^{2\mu_v + \sigma_v^2}(e^{\sigma_v^2} - 1). \end{aligned} \tag{12}$$

Finally, using the results obtained above, we further simplify Equation 11 and define the closed-form TDOA measurement model as

$$\begin{aligned} \tilde{p}_{uv}(\Delta\tau_{uv}) = \Big(&\mathrm{P}_{L_u}\mathrm{P}_{L_v}p_{\sqrt{2}\mathcal{N}} + \\ &\mathrm{P}_{L_u}(1-\mathrm{P}_{L_v})p_{\ln\mathcal{N},v}^- + \\ &\mathrm{P}_{L_v}(1-\mathrm{P}_{L_u})p_{\ln\mathcal{N},u} + \\ &(1-\mathrm{P}_{L_u})(1-\mathrm{P}_{L_v})p_{\tilde{\mathcal{N}}}\Big)(\Delta\tau_{uv}). \end{aligned} \tag{13}$$

Figure 2(b) shows an example of this model. Figure 2(c) describes the four terms in Eq. 13, and illustrates how they are interpreted as LOS-LOS, LOS-NLOS, NLOS-LOS, or NLOS-NLOS configurations for a pair of base stations.

In order to validate our approach, we performed a statistical comparison between the approximated and the general model. We note that, generally, the true UWB model parameter values lie in the ranges reported in Table I (confirmed by the experimental measurement campaigns performed in [1] and [12]). We first compared the approximation of $p_{\ln\mathcal{N},u} * p_{\ln\mathcal{N},v}^-$ with the normal density function $p_{\tilde{\mathcal{N}}}$ (defined by $\tilde{\mu}$ and $\tilde{\sigma}^2$ as in Equation 12). For the base station pair $\langle\mathcal{B}_u, \mathcal{B}_v\rangle$, we varied the parameters μ_u, μ_v and σ_u, σ_v of the respective log-normal distributions within the ranges shown in Table I so that 80'000 tests were performed.

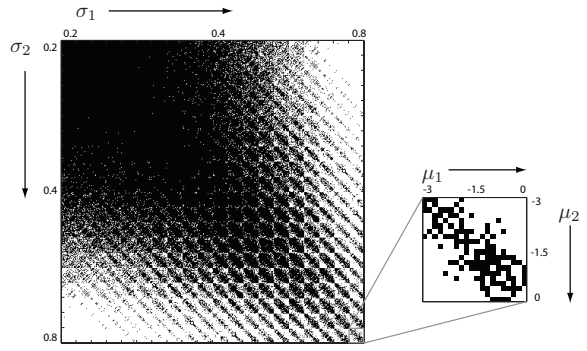

Fig. 3. Acceptance results of the Kolmogorov-Smirnov test at a 5% significance level, for 400^2 parameter variations (20 values for both μ_u and σ_u, in the ranges reported in Table I). Accepted tests are shown in black, rejected tests are shown in white.

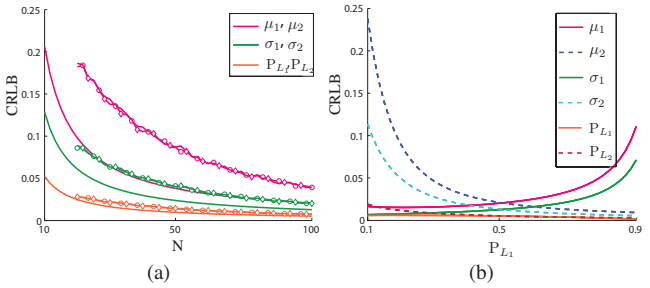

Fig. 4. CRLB for (a) a varying number of data samples N and (b) for varying LOS probability P_{L_1}, for default parameter values $\mu_{1,2} = -0.4$, $\sigma_{1,2} = 0.6$, and $\mathrm{P}_{L_{1,2}} = 0.5$. Additionally, (a) shows the average variance of the batch estimator detailed in Section IV-B, evaluated over 1000 runs. Symbols $\diamond$ and $\circ$ show parameter estimates for base station $\mathcal{B}_1$ and $\mathcal{B}_2$, respectively.

Figure 3 illustrates the acceptance results of the Kolmogorov-Smirnov test at a 5% significance level. The approximation clearly performs well for small σ_u, σ_v for all μ_u, μ_v, with an acceptance rate of 98.5% in the parameter range $\sigma_u, \sigma_v = [0.2, 0.55]$. Furthermore, for two base stations with similar NLOS behavior $|\sigma_u - \sigma_v| \leq 0.065$, the acceptance rate is 85.5% for all $\sigma_u, \sigma_v, \mu_u, \mu_v$. Secondly, we compared the full model (Equation 9) with the approximated model (Equation 13) over 800'000 tests measuring the Kolmogorov-Smirnov distance, for parameters $\sigma_u, \sigma_v, \mu_u, \mu_v, \mathrm{P}_{L_u}$ and P_{L_v} in the ranges as reported in Table I. The average Kolmogorov-Smirnov distance over all tests was 0.07, showing a good match of the densities.

III. Cramér-Rao Lower Bound

In this section, we calculate the Cramér-Rao lower bound (CRLB) for the efficient TDOA measurement model of Equation 13. The CRLB provides a lower bound on the variance of unbiased estimators and thereby provides a useful tool to assess the quality of algorithms which estimate the parameters of our model. Let us denote by $\hat{\tau}_{uv}^{(k)}$ the $k-$th measured TDOA value, and by N the total number of measured values. Given the associated true values $\tau_{uv}^{(k)}$, our data is $(\Delta\tau_{uv}^{(1)}, \Delta\tau_{uv}^{(2)}, ..., \Delta\tau_{uv}^{(N)})$. We consider the parameters of our measurement model

$$\boldsymbol{\theta} = [\mu_u, \sigma_u, \mu_v, \sigma_v, \mathrm{P}_{L_u}, \mathrm{P}_{L_v}]^{\mathsf{T}}$$

where we omit the measurement noise $\sigma_{\mathcal{N}}$, since it can easily be determined given an actual testbed. In order to determine the CRLB, we need to calculate the Fisher Information Matrix (FIM) $\mathbf{I}(\boldsymbol{\theta})$. Since the observations $\hat{\tau}_{uv}^{(k)}$ are independent, the FIM is then, by definition, the 6×6 matrix with entries

$$[\mathbf{I}(\boldsymbol{\theta})]_{i,j} := -\sum_{k=1}^{N} \mathrm{E}\left[\frac{\partial^2 \log \tilde{p}_{uv}(\Delta\tau_{uv}^{(k)}; \boldsymbol{\theta})}{\partial\theta_i \partial\theta_j}\right]. \quad (14)$$

Since the observations are identically distributed, we have

$$\begin{aligned}[\mathbf{I}(\boldsymbol{\theta})]_{i,j} =& -N\,\mathrm{E}\left[\frac{\partial^2 \log \tilde{p}_{uv}(\Delta\tau_{uv})}{\partial\theta_i \partial\theta_j}\right] \\ =& -N\int_{-\infty}^{0} \frac{\partial^2 \log \tilde{p}_{uv}(x)}{\partial\theta_i \partial\theta_j} \tilde{p}_{uv}(x)dx - \\ & N\int_{0}^{\infty} \frac{\partial^2 \log \tilde{p}_{uv}(x)}{\partial\theta_i \partial\theta_j} \tilde{p}_{uv}(x)dx. \end{aligned} \quad (15)$$

Recall that for fixed $x \in (0, \infty)$ we have

$$\begin{aligned}\tilde{p}_{uv}(x) =& \mathrm{P}_{L_u}\mathrm{P}_{L_v} p_{\sqrt{2}\mathcal{N}}(x) + \mathrm{P}_{L_v}(1-\mathrm{P}_{L_u}) p_{\ln\mathcal{N},u}(x) + \\ & (1-\mathrm{P}_{L_u})(1-\mathrm{P}_{L_v}) p_{\tilde{\mathcal{N}}}(x) \end{aligned} \quad (16)$$

and for $x \in (-\infty, 0)$ we have

$$\begin{aligned}\tilde{p}_{uv}(x) =& \mathrm{P}_{L_u}\mathrm{P}_{L_v} p_{\sqrt{2}\mathcal{N}}(x) + \mathrm{P}_{L_u}(1-\mathrm{P}_{L_v}) p_{\ln\mathcal{N},v}(-x) + \\ & (1-\mathrm{P}_{L_u})(1-\mathrm{P}_{L_v}) p_{\tilde{\mathcal{N}}}(x). \end{aligned} \quad (17)$$

Using Equation 17 for the first term and Equation 16 for the second term of Equation 15, it is now straightforward to deduce a closed-form expression for its integrand. Then, due to the complicated structure of this integrand, we are not able to perform the integration analytically but (for given $\boldsymbol{\theta}$) only numerically. Finally, for any unbiased estimator $\hat{\boldsymbol{\theta}} = (\hat{\theta}_1, ..., \hat{\theta}_6) = (\hat{\mu}_u, ..., \hat{P}_{L_v})$ for $\boldsymbol{\theta}$, we have the CRLB

$$\mathrm{Var}(\hat{\theta}_i) \geq [\mathbf{I}(\boldsymbol{\theta})^{-1}]_{i,i}. \quad (18)$$

Figure 4 shows the CRLB for our model and two base stations $\langle \mathcal{B}_1, \mathcal{B}_2 \rangle$, (a) for a varying number of data samples N, and (b) for a varying LOS probability P_{L_1}. As is to be expected, the CRLB decreases for increasing N. Also, we see that as P_{L_1} increases with respect to P_{L_2}, it becomes harder to estimate the log-normal parameters associated to the NLOS bias of base station $\mathcal{B}_1$.

IV. Estimation of Model Parameters

The application of the TDOA measurement model must be preceded by the estimation of its parameter vector $\boldsymbol{\theta}$, given measurement data $(\Delta\tau_{uv}^{(1)}, \Delta\tau_{uv}^{(2)}, ..., \Delta\tau_{uv}^{(N)})$, resulting in the model $\tilde{p}_{uv}(\Delta\tau_{uv}; \hat{\boldsymbol{\theta}})$. Due to its efficiency in achieving the CRLB for data set sizes tending to infinity, our approach is based on Maximum Likelihood Estimation (MLE). Although

several methods can be used to obtain the maximum likelihood estimate, we implement an Expectation Maximization (EM) approach, which, in contrast to other methods, does not require the evaluation of first and/or second derivatives of the likelihood function at each iteration. In our particular case, we will show that our EM formalism produces a compact, closed-form expression. In the following paragraphs, we detail an estimation framework that can be implemented offline (in batch mode) as well as online in real-time.

A. Preliminaries

The maximum likelihood estimator for our model is defined by

$$\hat{\boldsymbol{\theta}} = \arg\max_{\theta} \frac{1}{N} \sum_{k=1}^{N} \log \tilde{p}_{uv}(\Delta\tau_{uv}^{(k)}; \boldsymbol{\theta}). \tag{19}$$

Based on this estimator, the parameter vector $\boldsymbol{\theta}$ can be estimated offline by using the standard EM algorithm introduced by Dempster et al. [5]. Since our online approach builds upon the EM formalism presented by Cappé et al. [4], our notation in the following derivations is closely related to that of the latter. If we write our parameter vector $\boldsymbol{\theta}$ as

$$\boldsymbol{\theta} = [\mu_u, \sigma_u, \mu_v, \sigma_v, \tilde{\mu}, \tilde{\sigma}, \mathrm{P}_{L_u}, \mathrm{P}_{L_v}]^\mathsf{T}$$

where we introduce $\tilde{\mu}$ and $\tilde{\sigma}$ in order to resolve inter-parameter dependencies, we can formulate the four terms of our model as

$$\begin{aligned}
f_1(x;\boldsymbol{\theta}) &= p_{\sqrt{2}\mathcal{N}}(x;\boldsymbol{\theta}) = p_{\sqrt{2}\mathcal{N}}(x) \\
f_2(x;\boldsymbol{\theta}) &= p^{-}_{\ln\mathcal{N},v}(x;\boldsymbol{\theta}) = p^{-}_{\ln\mathcal{N},v}(x;\mu_v,\sigma_v) \\
f_3(x;\boldsymbol{\theta}) &= p_{\ln\mathcal{N},u}(x;\boldsymbol{\theta}) = p_{\ln\mathcal{N},u}(x;\mu_u,\sigma_u) \\
f_4(x;\boldsymbol{\theta}) &= p_{\tilde{\mathcal{N}}}(x;\boldsymbol{\theta}) = p_{\tilde{\mathcal{N}}}(x;\tilde{\mu},\tilde{\sigma}).
\end{aligned} \tag{20}$$

By defining $\alpha_1 = \mathrm{P}_{L_u}\mathrm{P}_{L_v}$, $\alpha_2 = \mathrm{P}_{L_u}(1-\mathrm{P}_{L_v})$, $\alpha_3 = \mathrm{P}_{L_v}(1-\mathrm{P}_{L_u})$, and $\alpha_4 = (1-\mathrm{P}_{L_u})(1-\mathrm{P}_{L_v})$, we can rewrite the model $\tilde{p}_{uv}$ in the form of a standard mixture model

$$\tilde{p}_{uv}(x;\boldsymbol{\theta}) = \sum_{j=1}^{4} \alpha_j f_j(x;\boldsymbol{\theta}). \tag{21}$$

Thus, we can now leverage the EM estimation framework for mixture models by assuming that every observation $\Delta\tau_{uv}^{(k)}$ originates from an f_j, and by postulating the existence of a latent variable $\mathbf{Z} = (Z_1, ..., Z_N)$ where $Z_k = j$ with probability α_j and $j \in \{1,2,3,4\}$. Z_k specifies which f_j the k-th observation corresponds to, thus, given $Z_k = j$, the observation $\Delta\tau_{uv}^{(k)}$ has density f_j. In other words, any given data sample corresponds to the probability density defined by two base stations in either LOS-LOS, NLOS-NLOS, or LOS-NLOS (and NLOS-LOS) configuration. For any k, the likelihood of $(\Delta\tau_{uv}^{(k)}, Z_k)$ is

$$f(x,z;\boldsymbol{\theta}) = \sum_{j=1}^{4} \alpha_j \delta_{zj} f_j(x;\boldsymbol{\theta})$$

with $\delta_{zj} = 1$ if $z = j$ and $\delta_{zj} = 0$ otherwise. Note that here (and in what follows) there is no dependency on k, since the observations are i.i.d. We are now able to write f in exponential family form:

$$\begin{aligned}
f(x,z;\boldsymbol{\theta}) &= h(x,z)\exp\left(\sum_{j=1}^{4}\delta_{zj}[\log(\alpha_j) + \log(f_j(x;\boldsymbol{\theta}))]\right) \\
&= h(x,z)\exp\left(\sum_{j=1}^{11} S_j(x,z)\phi_j(\boldsymbol{\theta})\right)
\end{aligned} \tag{22}$$

where $h(x,z) = 0$ if $z = 2$ and $x \geq 0$, or $z = 3$ and $x \leq 0$, and $h(x,z) = 1$ otherwise. $S = (S_1, ..., S_{11})$ and $\phi = (\phi_1, ..., \phi_{11})$ are defined as follows:

$$\begin{aligned}
S(x,z) = [&\delta_{z,1},\ x^2\delta_{z,1},\ \chi_{(-\infty,0)}(x)\delta_{z,2}, \\
&\chi_{(-\infty,0)}(x)\log(-x)\delta_{z,2}, \\
&\chi_{(-\infty,0)}(x)\log(-x)^2\delta_{z,2},\ \chi_{(0,\infty)}(x)\delta_{z,3}, \\
&\chi_{(0,\infty)}(x)\log(x)\delta_{z,3},\ \chi_{(0,\infty)}(x)\log(x)^2\delta_{z,3}, \\
&\delta_{z,4},\ x\delta_{z,4},\ x^2\delta_{z,4}]^\mathsf{T}
\end{aligned} \tag{23}$$

$$\begin{aligned}
[\phi_1,\phi_2]^\mathsf{T}(\boldsymbol{\theta}) &= \left[\log(\alpha_1) - \log(2\sqrt{\pi}\sigma),\ -\frac{1}{4\sigma_{\mathcal{N}}^2}\right]^\mathsf{T} \\
[\phi_3,\phi_4,\phi_5]^\mathsf{T}(\boldsymbol{\theta})) &= \left[-\log(2\sqrt{\pi}\sigma_v) + \log(\alpha_2) - \frac{\mu_v^2}{2\sigma_v^2},\right. \\
&\qquad \left. -1 + \frac{\mu_v}{\sigma_v^2}, -\frac{1}{2\sigma_v^2}\right]^\mathsf{T} \\
[\phi_6,\phi_7,\phi_8]^\mathsf{T}(\boldsymbol{\theta})) &= \left[-\log(2\sqrt{\pi}\sigma_u) + \log(\alpha_3) - \frac{\mu_u^2}{2\sigma_u^2},\right. \\
&\qquad \left. -1 + \frac{\mu_u}{\sigma_u^2}, -\frac{1}{2\sigma_u^2}\right]^\mathsf{T} \\
[\phi_9,\phi_{10},\phi_{11}]^\mathsf{T}(\boldsymbol{\theta}) &= \left[-\log(2\sqrt{\pi}\tilde{\sigma}) + \log(\alpha_4) - \frac{\tilde{\mu}^2}{2\tilde{\sigma}^2},\right. \\
&\qquad \left. \frac{\tilde{\mu}}{\tilde{\sigma}^2}, -\frac{1}{2\tilde{\sigma}^2}\right]^\mathsf{T}
\end{aligned} \tag{24}$$

where $\chi_{[.]}$ is the indicator function for a given interval. We denote by $\mathrm{E}_{\boldsymbol{\theta}}[\cdot|\Delta\tau_{uv}^{(k)} = x]$ the expectation given $\Delta\tau_{uv}^{(k)} = x$ and $\boldsymbol{\theta}$, and define weights $\bar{w}_j(x;\boldsymbol{\theta})$ obtained through Bayes' theorem as

$$\begin{aligned}
\bar{w}_j(x;\boldsymbol{\theta}) &:= \mathrm{E}_{\boldsymbol{\theta}}[\delta_{jZ_k}|\Delta\tau_{uv}^{(k)} = x] \\
&= \frac{\alpha_j f_j(x;\boldsymbol{\theta})}{\sum_{m=1}^{4}\alpha_m f_m(x;\boldsymbol{\theta})}
\end{aligned} \tag{25}$$

which is equal to the probability that $Z_k = j$ given $\Delta\tau_{uv}^{(k)} = x$. Then for $\bar{s}(x;\boldsymbol{\theta}) := \mathrm{E}_{\boldsymbol{\theta}}[S(\Delta\tau_{uv}^{(k)}, Z_k)|\Delta\tau_{uv}^{(k)} = x]$ we have

$$\begin{aligned}
\bar{s}(x;\boldsymbol{\theta}) = [&w_1(x;\boldsymbol{\theta}),\ w_1(x;\boldsymbol{\theta})x^2,\ w_2(x;\boldsymbol{\theta}), \\
&w_2(x;\boldsymbol{\theta})\log(-x),\ w_2(x;\boldsymbol{\theta})\log(-x)^2, \\
&w_3(x;\boldsymbol{\theta}),\ w_3(x;\boldsymbol{\theta})\log(x),\ w_3(x;\boldsymbol{\theta})\log(x)^2, \\
&w_4(x;\boldsymbol{\theta}),\ w_4(x;\boldsymbol{\theta})x,\ w_4(x;\boldsymbol{\theta})x^2]^\mathsf{T}.
\end{aligned} \tag{26}$$

Finally, for $s \in \mathbb{R}^{11}$ we define the function $l(s;\boldsymbol{\theta}) = \sum_{j=1}^{11} s_j\phi_j(\boldsymbol{\theta})$. Through straightforward

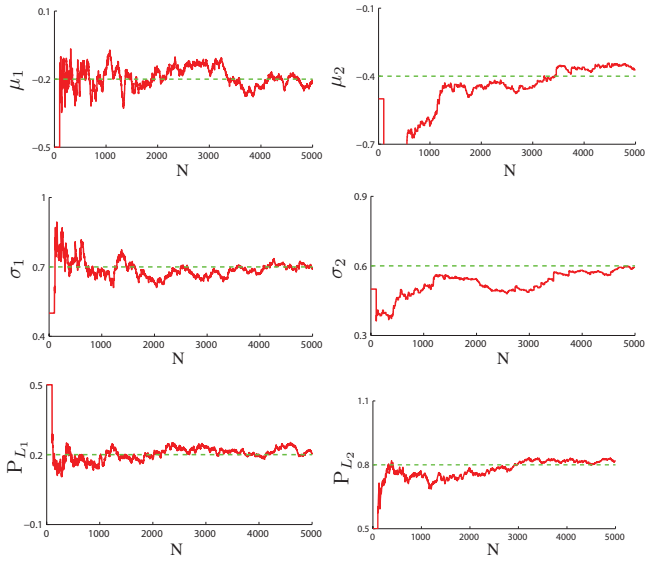

Fig. 5. Online EM estimation of model parameters for a base station pair $\langle \mathcal{B}_1, \mathcal{B}_2 \rangle$, with true values $\mu_1 = -0.2$, $\mu_2 = -0.4$, $\sigma_1 = 0.7, \sigma_2 = 0.6$, $P_{L_1} = 0.2$, $P_{L_2} = 0.8$, for $N = 5000$ data samples and $\gamma = 1/k^{0.65}$. Parameters $\tilde{\mu}$ and $\tilde{\sigma}$ (not shown here) are defined as in Eq. 12, to form the full parameter vector $\boldsymbol{\theta}$.

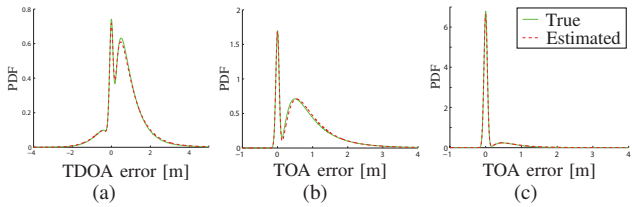

Fig. 6. Superimposed true and estimated probability densities, for values of $\boldsymbol{\theta}$ and $\hat{\boldsymbol{\theta}}$ as shown in Figure 5. (a) $\tilde{p}_{12}(\Delta\tau_{12})$ (b) $\tilde{p}_1(\Delta r_1)$ and (c) $\tilde{p}_2(\Delta r_2)$

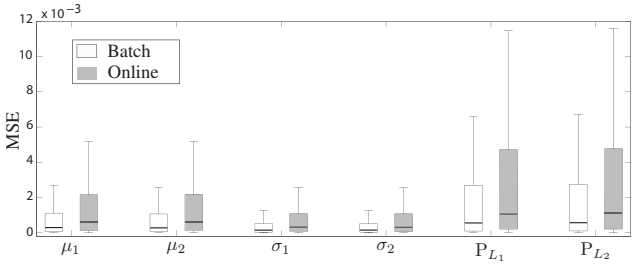

Fig. 7. The graphs shows boxplots of the mean-squared-error $(\boldsymbol{\theta}_i - \hat{\boldsymbol{\theta}}_i)^2$, with $\hat{\boldsymbol{\theta}}$ resulting from the batch and the online estimation algorithms. The boxplot edges mark the 25th and 75th percentiles, the bar marks the median, and the whiskers cover 99.3% of the data.

calculation we can derive conditions on s so that we can define the function $\bar{\boldsymbol{\theta}}(s) := \arg\max_{\boldsymbol{\theta}} l(s;\boldsymbol{\theta})$, which leads to

$$\bar{\boldsymbol{\theta}}(s) = \left[\frac{s_7}{s_6}, \sqrt{\frac{-s_7^2 + s_6 s_8}{s_6^2}}, \frac{s_4}{s_3}, \sqrt{\frac{-s_4^2 + s_3 s_5}{s_3^2}}, \right.$$
$$\frac{s_{10}}{s_9}, \sqrt{\frac{-s_{10}^2 + s_9 s_{11}}{s_9^2}}, \frac{s_1 + s_3}{s_1 + s_3 + s_6 + s_9},$$
$$\left. \frac{s_1 + s_6}{s_1 + s_3 + s_6 + s_9} \right]^{\mathsf{T}}. \tag{27}$$

We note that Equations 25 and 26 relate to the E-step and that Equation 27 relates to the M-step of a standard, batch EM algorithm. As we will see below, the implementations of the batch and online algorithms now only require the evaluation of these closed-form vectors.

B. Batch Estimation

Using the notations introduced above, for N data samples, the $k+1$-th parameter estimate $\hat{\boldsymbol{\theta}}^{(k+1)}$ in the batch EM algorithm is given by

$$\hat{\boldsymbol{\theta}}^{(k+1)} = \bar{\boldsymbol{\theta}} \left(\frac{1}{N} \sum_{i=1}^{N} \bar{s}(\Delta\tau_{uv}^{(i)}; \hat{\boldsymbol{\theta}}^{(k)}) \right). \tag{28}$$

Figure 4 (a) shows how, as expected, the estimator variance tends towards the CRLB for $N \to \infty$, confirming its efficiency for growing N.

C. Online Estimation

The $k+1$-th parameter estimate $\hat{\boldsymbol{\theta}}^{(k+1)}$ for observations $(\Delta\tau_{uv}^{(1)}, ..., \Delta\tau_{uv}^{(k)})$ takes the form

$$\hat{s}^{(k+1)} = \hat{s}^{(k)} + \gamma^{(k+1)} \left[\bar{s} \left(\Delta\tau_{uv}^{(k+1)}; \hat{\boldsymbol{\theta}}^{(k)} \right) \right) - \hat{s}^{(k)} \Big]$$
$$\hat{\boldsymbol{\theta}}^{(k+1)} = \bar{\boldsymbol{\theta}}(\hat{s}^{(k+1)}) \tag{29}$$

where $\gamma^{(k+1)}$ is a user-defined step size. Variations of $\gamma^{(k)} = 1/k$ have shown to produce good convergence speed [4] – typically, the choice γ defines the trade-off between adaptability and stability of the estimate. In practice, one should bound γ from below to allow the estimation algorithm to continuously adapt to a changing environment. Since the second and third term of our mixture model are defined by densities that are only supported on a semi-infinite interval, we do not update the entries of $\hat{s}_{3,4,5}^{(k+1)}$ when $\Delta\tau_{uv}^{(k+1)} \in (0, \infty)$ and similarly of $s_{6,7,8}^{(k+1)}$ when $\Delta\tau_{uv}^{(k+1)} \in (-\infty, 0)$. Also, we use Equation 12 for calculating $\tilde{\mu}$ and $\tilde{\sigma}$ in function of the parameter estimates $\hat{\mu}_1$, $\hat{\mu}_2$, $\hat{\sigma}_1$, and $\hat{\sigma}_2$, instead of $\bar{\boldsymbol{\theta}}(\hat{s}^{(k+1)})_{5,6}$, since the convergence speed is significantly improved.

Figure 5 shows an example of online parameter estimation using our EM framework, on a data set comprising 5000 samples. Cappé et al. [4] resolve issues due to the dependency on the initialization by updating only $\hat{s}$ for a number of first iterations. Thus, we use the first 100 observations to build up an estimate of $\hat{s}^{(100)}$, before calculating the first parameter estimate $\hat{\theta}^{(101)}$. Figure 6 shows the true probability densities superimposed by the (final) estimated probability densities of the online estimation example shown in Figure 5. The plots confirm, qualitatively, that a good estimation is achieved. Figure 7 shows a systematic comparison of the batch with the online estimation algorithm. We performed a

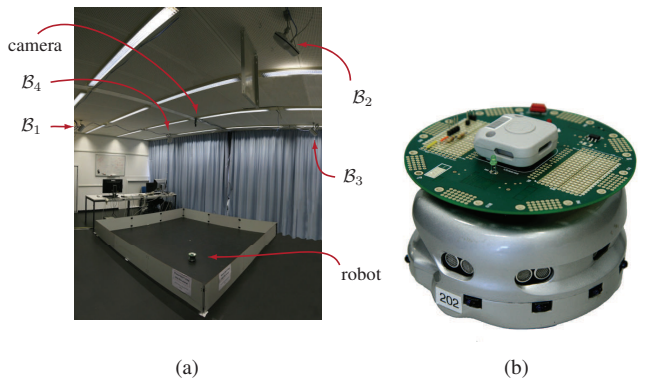

(a) (b)

Fig. 8. (a) Experimental setup, including a 3m×3m arena, an overhead camera tracking system, and 4 UWB base station receivers mounted on the ceiling. Base station $\mathcal{B}_2$ is occluded by a metal sheet to provoke a NLOS scenario. (b) Khepera III robot equipped with a LED-based tracking module, which simultaneously carries the UWB emitter tag.

set of 10'000 simulations, where for each simulation, true parameters $\boldsymbol{\theta}$ were sampled randomly in the intervals as reported in Table I. Both algorithms were tested on a sample size $N = 1000$, where, for the online algorithm, the final estimate of $\hat{\boldsymbol{\theta}}$ is found by averaging the last 100 estimates. The results confirm good estimation of the model parameters. As is to be expected, the batch algorithm produces slightly smaller estimation errors than the online algorithm.

V. Experiments

Our experimental setup is shown in Figure 8(a). The UWB localization system employed in this work is commercially available from Ubisense [1], Series 7000 (sensors and compact tags). It is installed on the ceiling of a 40m^2 laboratory, with each of the four base stations mounted at the extremities of a 9m^2 square robotic arena. To perform experiments, we use a Khepera III robot, which is a differential drive robots of 12cm diameter produced by K-Team corporation[2], see Figure 8(b). The robot uses wheel encoders to provide odometry readings (the dead-reckoning error of the Khepera III has been reported to reach 0.1m after traveling for 18 meters [11].) The Khepera III robot has a KoreBot extension board providing a standard embedded Linux operating system on an Intel XSCALE PXA-255 processor running at 400 MHz. Communication is enabled through an IEEE 802.11b wireless card which is installed in a built-in CompactFlash slot. The robot is equipped with an LED ground-truth position tracking module, which also carries a Ubisense UWB emitter tag. To measure ground truth positioning, an overhead camera system is installed over the arena in combination with the open source tracking software *Swis-Track* [10]. The maximum error of the resulting ground truth positioning is below 3cm (as reported in [11]). Odometry updates are made at a frequency of 5Hz, the UWB tags emit positioning pulses at an update frequency of about 1Hz, and the overhead camera tracks the robot at 10Hz. In order to

[1]http://www.ubisense.net
[2]http://www.k-team.com/

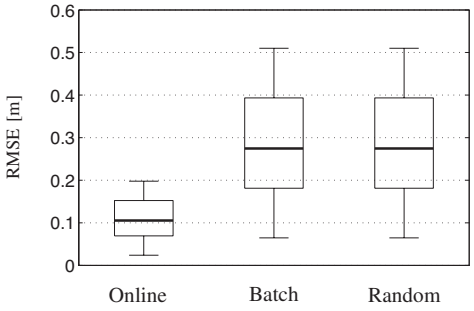

Fig. 9. Experimental results obtained from data gathered on the real setup (the performance is shown by the root-mean-square-error, in meters). Evaluations were performed on three model variants: *(i)* online model estimation, *(ii)* batch model estimation, and *(iii)* random model. The boxplots show the 25th, 50th, and 75th percentile, and the whiskers contain 85% of the data.

provoke a partial NLOS setting, we suspend a metal sheet in front of base station $\mathcal{B}_2$ (as seen in Figure 8(a)), which occludes the LOS signal path from the robot for certain localities. Using this setup, we perform experiments of 50 minutes duration, during which the robot (driving at 12 cm/s) is able to fully cover the arena. We collect synchronized data consisting of unfiltered UWB TDOA measurements for three base station pairs, robot odometry measurements, and ground truth positioning information from the overhead camera, which we use to build a dataset of $\Delta\tau^{(k)}$ values, and $k \leq N = 1600$. The robot runs a particle filter localization algorithm (with a set of 100 particles), which employs a standard motion model based on odometry readings, and the UWB measurement model described in this paper (apart from these two modalities, the robot employs no other sensors). We test the performance of this localization algorithm over 500 evaluations on our dataset, for the following 3 scenarios:

Online We use $\tilde{p}_{uv}(\Delta\tau_{uv}; \hat{\boldsymbol{\theta}}^{(\boldsymbol{k-1})})$ for localization. The measurement model is then re-evaluated for each new incoming data sample $\Delta\tau_{uv}^{(k)}$, using the online expression (Eq. 29) with the practical considerations explained in Sec. IV-C. We set $\gamma^{(k)} = 0.45$ to ensure adaptability.

Batch The model is calculated a priori for all data at once using the batch expression (Eq. 28), iterated $M = 40$ times (leading to convergence). At all times, we use $\tilde{p}_{uv}(\Delta\tau_{uv}; \hat{\boldsymbol{\theta}}^{(M)})$.

Random A random model is defined a priori, with parameter values $\hat{\boldsymbol{\theta}}_{\text{rand}}$ sampled randomly in the intervals reported in Table I. At all times, we use $\tilde{p}_{uv}(\Delta\tau_{uv}; \hat{\boldsymbol{\theta}}_{\text{rand}})$.

We discuss the localization performance in terms of the mean positioning error (RMSE, in meters) of all particles in the robot's belief, a metric which implicitly includes the spread (or variance) of the particle positions. Figure 9 shows the distribution of the localization errors throughout the experiments in form of boxplots for all scenarios. We note that for our experimental setup, odometry by itself would reach an error of about 1.6m. We also note that if we were to calculate the positions by resolving the trilateration problem (given the TDOA data) via maximum likelihood estimates, the mean localization error would amount to 0.66m (quantifying the poor quality of the TDOA measurement data).

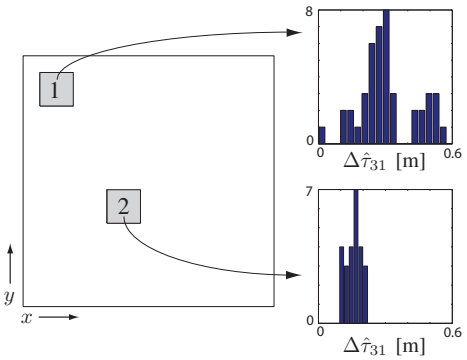

Fig. 10. Histogram plots of TDOA measurements gathered in our experiments for base station pair $\langle \mathcal{B}_3, \mathcal{B}_1 \rangle$, for two distinct areas in our experimental arena. The areas are delimited by the ranges $X_1 = (0.2, 0.6)$, $Y_1 = (2.4, 2.8)$, $X_2 = (1, 1.4)$, $Y_2 = (1, 1.4)$.

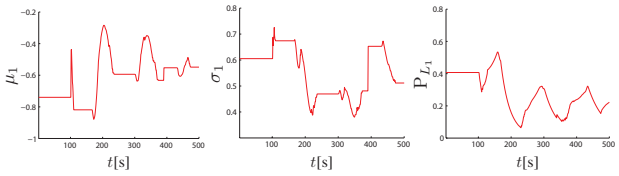

Fig. 11. Development of parameter estimates over time, for base station $\mathcal{B}_1$, of the online estimation algorithm for an experimental run in our real robotic setup.

Our results show that the online model estimation leads to a localization performance improved by a factor of almost 3 (with an average error of 0.1m) with respect to the batch model estimate and the random model. Furthermore, the robustness of this method is indicated by the small spread of the localization errors. Due to the fact that LOS/NLOS path conditions are defined by the physical environment, certain localities may produce measurements with large biases with a greater probability than other localities. This artifact is illustrated in Figure 10, where we clearly see how two distinct localities produce very different error statistics. As a result, the performance of the batch method and the random methods are quite similar, since both models assume non-spatiality by using a single, a priori determined error model over the whole space.

Finally, we conclude that the online estimation algorithm is able to capture the spatiality of the UWB signal path by adapting its estimate to recent data samples. The adaptive behavior of the model can be observed in Figure 11, where we show the development of parameter estimates over time, for base station $\mathcal{B}_1$.

VI. Conclusion

This work is situated in the context of on-board UWB TDOA localization in mixed LOS/NLOS positioning scenarios. We consider a general UWB range model, and propose a closed-form approximation which is validated for model parameter values that are specific to UWB signals in indoor environments. We address the problem of estimating the parameters of this new model using the ML estimator. Considering the similarity of our model and a mixture model, the EM estimation algorithm takes a simple form. Moreover, we are able to derive an elegant online estimation algorithm. Experimental results on a mobile robot equipped with an UWB emitter show excellent localization performance when employing the online model estimation in real-time. Through its adaptive nature, the online estimation algorithm ultimately enables the measurement model to capture the spatiality of LOS/NLOS path conditions over time, and thus proves to be a promising tool for localization in indoor environments.

References

[1] N. Alsindi, B. Alavi, and K. Pahlavan. Measurement and Modeling of Ultrawideband TOA-Based Ranging in Indoor Multipath Environments. *IEEE Transactions on Vehicular Technology*, 58:1046–1058, 2009.

[2] G. Benet, F. Blanes, J. E. Simo, and P. Perez. Using infrared sensors for distance measurement in mobile robots. *Robotics and Autonomous Systems*, 40(4):255–266, 2002.

[3] M. Betke and L. Gurvits. Mobile robot localization using landmarks. *IEEE Transactions on Robotics and Automation*, 13(2):251–263, 1997.

[4] O. Cappe and E. Moulines. On-line expectation-maximization algorithm for latent data models. *Journal of the Royal Statistical Society. Series B (Methodological)*, 71:593–613, 2009.

[5] A. P. Dempster, N. M. Laird, and D. B. Rubin. Maximum likelihood from incomplete data via the EM algorithm. *Journal of the Royal Statistical Society. Series B (Methodological)*, 39(1):1–38, 1977.

[6] J. Gonzalez, J. L. Blanco, C. Galindo, A. Ortiz-de Galisteo, J. A. Fernandez-Madrigal, F. A. Moreno, and J. L. Martinez. Mobile robot localization based on Ultra-Wide-Band ranging: A particle filter approach. *Robotics and Autonomous Systems*, 57(5):496–507, 2009.

[7] D. Jourdan, J. J. Deyst, M. Win, and N. Roy. Monte Carlo localization in dense multipath environments using UWB ranging. In *IEEE International Conference on Ultra-Wideband (ICU)*, pages 314–319, 2005.

[8] J. J. Leonard and H. F. Durrant-Whyte. *Directed Sonar Sensing for Mobile Robot Navigation*. Kluwer Academic Publishers, 1992.

[9] H. Liu, H. Darabi, P. Banerjee, and J. Liu. Survey of Wireless Indoor Positioning Techniques and Systems. *IEEE Transactions on Systems, Man and Cybernetics*, 37(6):1067–1080, 2007.

[10] T. Lochmatter, P. Roduit, C. Cianci, N. Correll, J. Jacot, and A. Martinoli. SwisTrack - A Flexible Open Source Tracking Software for Multi-Agent Systems. In *Proceedings of the 2008 IEEE/RSJ International Conference on Intelligent Robots and Systems*, pages 4004–4010, 2008.

[11] A. Prorok, A. Arfire, A. Bahr, J. R. Farserotu, and A. Martinoli. Indoor navigation research with the Khepera III mobile robot: An experimental baseline with a case-study on ultra-wideband positioning. In *International Conference on Indoor Positioning and Indoor Navigation (IPIN)*, 2010. doi: 10.1109/IPIN.2010.5647880.

[12] A. Prorok, P. Tomé, and A. Martinoli. Accommodation of NLOS for Ultra-Wideband TDOA Localization in Single- and Multi-Robot Systems. In *International Conference on Indoor Positioning and Indoor Navigation (IPIN)*, 2011. doi: 10.1109/IPIN.2011.6071927.

[13] Y. Qi. *Wireless geolocation in a non-line-of-sight environment*. PhD thesis, Princeton University, 2004.

[14] Z. Sahinoglu, S. Gezici, and I. Guvenc. *Ultra-wideband Positioning Systems. Theoretical Limits, Ranging Algorithms, and Protocols*. Cambridge University Press, 2008.

[15] M. Segura, H. Hashemi, C. Sisterna, and V. Mut. Experimental demonstration of self-localized Ultra Wideband indoor mobile robot navigation system. In *International Conference on Indoor Positioning and Indoor Navigation (IPIN)*, 2010. doi: 10.1109/IPIN.2010.5647457.

[16] S. Thrun, M. Bennewitz, W. Burgard, A. Cremers, F. Dellaert, D. Fox, D. Hahnel, C. Rosenberg, N. Roy, J. Schulte, and D. Schulz. MINERVA: a second-generation museum tour-guide robot. In *Proceedings of the 1999 IEEE International Conference on Robotics and Automation*, pages 1999–2005, 1999.

[17] S. Thrun, W. Burgard, and D. Fox. A real-time algorithm for mobile robot mapping with applications to multi-robot and 3D mapping. In *Proceedings of the IEEE International Conference on Robotics and Automation (ICRA)*, pages 321–328, 2000.